**Steel and Composite Structures**, *Vol. 33, No. 6* (*2019*) *849-864*
DOI: https://doi.org/10.12989/scs.2019.33.6.849


# Compressive and flexural behaviors of ultra-high strength concrete encased steel members

Yong Du [1,2], Ming-Xiang Xiong [*3,2], Jian Zhu [1] and J.Y. Richard Liew [2]

[1] *College of Civil Engineering*, *Nanjing Tech University*, *Nanjing*, *China*
[2] *Department of Civil and Environmental Engineering*, *National University of Singapore*, *117576*, *Singapore*
[3] *Protective Structures Centre*, *School of Civil Engineering*, *Guangzhou University*, *Guangzhou*, *China*

(*Received August 8, 2019, Revised November 1, 2019, Accepted November 20, 2019*)

**Abstract.** One way to achieve sustainable construction is to reduce concrete consumption by use of more sustainable and higher strength concrete. Modern building codes do not cover the use of ultra-high strength concrete (UHSC) in the design of composite structures. Against such background, this paper investigates experimentally the mechanical properties of steel fibre-reinforced UHSC and then the structural behaviors of UHSC encased steel (CES) members under both concentric and eccentric compressions as well as pure bending. The effects of steel-fibre dosage and spacing of stirrups were studied, and the applicability of Eurocode 4 design approach was checked. The test results revealed that the strength of steel stirrups could not be fully utilized to provide confinement to the UHSC. The bond strength between UHSC and steel section was improved by adding the steel fibres into the UHSC. Reducing the spacing of stirrups or increasing the dosage of steel fibres was beneficial to prevent premature spalling of the concrete cover thus mobilize the steel section strength to achieve higher compressive capacity. Closer spacing of stirrups and adding 0.5% steel fibres in UHSC enhanced the post-peak ductility of CES columns. It is concluded that the code-specified reduction factors applied to the concrete strength and moment resistance can account for the loss of load capacity due to the premature spalling of concrete cover and partial yielding of the encased steel section.

**Keywords:** concrete encased steel column; ultra-high strength concrete; steel fibres; compressive/flexural/beam-column behaviors; plastic design approach; ductility

## 1. Introduction

Steel-concrete composite columns have gained its popularity in modern high-rise buildings due to their superior performance in terms of high load capacity, fast-track construction, lesser environmental impact, and cost-saving. Moreover, the high stiffness of the CES columns has a beneficial effect to control the lateral deflection of high-rise buildings when they are used in lateral load resisting system (Begum *et al*. 2013). There are some design codes worldwide catering for the design of CES columns. However, the concrete strength is limited, for instance, the cylinder concrete strength is limited to 67 N/mm$^2$ in Chinese Code (GB 50936 2014), 50 N/mm$^2$ in Eurocode 4 (EN 1994-1-1 2004), and 70 N/mm$^2$ in American code (ANSI/AISC 360 2016), respectively. Higher strength concrete such as the ultra-high strength concrete (UHSC, $f_{ck}$ > 90 MPa) (Liew and Xiong 2015) is not allowed due to some common concerns on its quality inconsistency (Sharmila and Dhinakaran 2015), spalling under fire (Xiong and Liew 2016) and poor ductility (Pons *et al*. 2018). Currently, UHSC is attractive for sustainable construction as it reduces the use of concrete materials. As the concreting technology develops, the quality of UHSC can be ensured (Liew and Xiong 2015), its spalling problem can be overcome (Xiong and Liew 2015), and the ductility can be improved (El-Tawil and Deierlein 1999, Naito et al. 2011). For these reasons, the CES columns with the UHSC can be recommended, especially for high-rise buildings, provided the design provisions are available. To explore the use of UHSC in structural elements to handle high-stress levels in high-rise buildings is one of the motivations of this research.

For normal strength CES members, the design provisions are available as mentioned in above building codes. Generally, they are based on plastic design method. In other words, the plastic resistance to compression or bending moment can be achieved at ultimate limit state. However, this is not sure for CES columns with the UHSC. Xiong *et al*. have conducted a series of experimental work on compressive (Xiong *et al*. 2017a), flexural (Xiong *et al*. 2017b), and beam-column (Xiong *et al*. 2017c) behaviors of the concrete filled steel tubular (CFST) columns using UHSC with strength up to 200 MPa. Their study concluded that the plastic design method could be adopted but the code-specified confinement effect should be ignored. Although the confinement effect is ignored, the beneficial effect of confining stress from the tube to suppress the concrete cracks exists, this is helpful to achieve the plastic resistance of the CFST members. However, for the CES members with the UHSC, the confinement action of stirrups may be minimal except for the CES columns using circular

∗Corresponding author, Associate Professor,
E-mail: cvexmx@gzhu.edu.cn


http://www.techno-press.org/?journal=scs&subpage=6
ISSN: 1229-9367 (Print), 1598-6233 (Online)

or spiral stirrups. Besides, the global or local buckling of the encased steel section may create premature cracks of concrete cover. Also, the encased steel section may not fully yield under pure bending in cases where it is placed far away from the edge of cross-section. These are factors adverse to achieve plastic resistance. In these regards, a new reduction factor may be needed to consider the premature cracks of concrete and partial yielding of steel, similar to the CES columns with the normal strength concrete (NSC) in Eurocode 4 (EN 1994-1-1 2004). To check the applicability of current design approach and provide proper design recommendations is another motivation of this study.

There have been some studies concerning the structural behavior of CES members employing high strength concrete (HSC) and UHSC from different perspectives. Zhu *et al.*'s (2014) study on the axial compressive behavior of short CES columns revealed that the stirrups contributed to the improvement of ductility but not the load capacity, this indicated that the confinement was limited to improve the strength of concrete up to 94 MPa (cylinder strength). *Kim et al*. (2012 and 2014) carried out a series of tests to investigate the axial load-bending moment relationship of medium to slender CES columns under the eccentric loads. The cylinder compressive strength of concrete was 94 MPa, 104 MPa, 113 MPa, and 184 MPa. It was found that the ACI 318-08 (2008) underestimated the load capacity by neglecting the confinement effect; whereas the Eurocode 4 (EN 1994-1-1 2004) and AIJ (2001) overestimated the test results by using plastic stress distribution. The overestimation might be due to the encased high strength steel column whose plastic resistance was not achieved. Modifications to current design provisions with plastic design methods were thus needed but unfortunately not provided in their research. On the contrary, Lai *et al.*'s (2019) study showed that the Eurocode 4 and AISC approaches provided conservative but safe estimations on the buckling resistance of slender CES columns with concrete grade up to C100. This means there is a disagreement existing in the literature regarding the design method for the CES members using high strength materials. Hence, more relevant studies are needed to clarify the disagreement. There are also other studies conducted for the shear capacity (Xue *et al*. 2012, Yao *et al*. 2014), performance under hazards (Ricles and Paboojian 1994, Zhu *et al*. 2016, 2017, Choi *et al*. 2012), and numerical modelling (Begum *et al*. 2013, Ellobody and Young 2011, Kara and Dundar 2012, Kim and Hwang 2018) of the CES members with HSC or UHSC. Overall, the above-mentioned studies have indicated improved strength and stiffness of CES columns with UHSC as compared to those with NSC or HSC, demonstrated them as a promising type of composite members to handle high-stress levels.

However, the test data for CES members with the UHSC is still lesser than their counterparts with the NSC and HSC; and whether the plastic design method can be used is still in doubt. By understanding the compressive strength, bending moment resistance, and axial load - bending moment interactive strength are only related with their cross-sectional geometries and material properties, a comprehensive test program has been designed in this study to investigate their compressive behavior with short columns taking concentric compression, pure flexural resistance with longitudinal beams under two-point load, and cross-sectional *M-N* interactive strength with short columns subjected to eccentric compression. The design of such a test program was aiming to eliminate the second-order effect from the geometric imperfection where usually exists in slender columns. The cubic strength of the UHSC was in a range of 100 MPa to 140 MPa, exceeding the limits of current design codes such as Chinese Code (GB 50936 2014), Eurocode 4 (EN 1994-1-1 2004), and American code (ANSI/AISC 360 2016), etc. Steel fibres were used as they are deemed to improve ductility of the UHSC (Gao *et al*. 2018). The failure modes, ductility, and calculations on the load capacities (i.e., axial, flexural and beam-column capacities) were presented and discussed. This study has clarified the disagreement existing in the available literature and solved the problem of designing CES members with UHSC up to 140 MPa (cubic strength).

Table 1 Specimen details

| Group | Specimen ID | Sizes (*mm*) ($b \times h \times L$) | Concrete strength (MPa) | Elasticity of modulus (GPa) | Cover thickness ($c$, *mm*) | Spacing of stirrups ($s$, *mm*) | Steel fibre in volume, *SF* (%) | Load eccentricity (*mm*) |
|---|---|---|---|---|---|---|---|---|
| A | GJ-1 | 300×300×840 | 104.2 | 44.7 | 25 | 100 | 0 | 0 |
| | GJ-2 | | 102.6 | 44.5 | 15 | 100 | | |
| | GJ-3 | | 115.2 | 46.2 | | 75 | | |
| | GJ-4 | | 105.3 | 44.9 | | 50 | | |
| B | GJ-5 | 300×300×840 | 126.9 | 47.7 | 15 | 50 | 0.3 | 0 |
| | GJ-6 | | 130.3 | 48.2 | | | 0.4 | |
| | GJ-7 | | 135.7 | 48.8 | | | 0.5 | |
| C | GJ-8 | 300×300×840 | 134.6 | 48.7 | 15 | 50 | 0.5 | 35 |
| | GJ-9 | | 134.6 | 48.7 | | | | 125 |
| D | GJ-10 | 300×300×2400 | 134.6 | 48.7 | 15 | 50 | 0.5 | Bending |

*Note: The cover thickness refers to the distance from the surface of the specimen to the surface of the stirrup

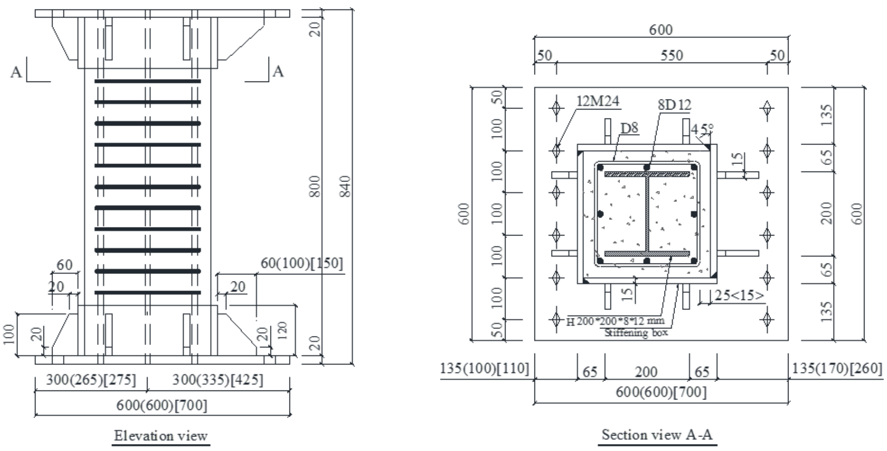


*Notes: Values in "( )" are for specimens with 35 *mm* load eccentricity; and values in "[ ]" are for specimens with 125 *mm* load eccentricity. For the cover thickness, the value in "< >" is applicable to all specimens except GJ-1

Fig. 1 Details of test specimens (unit: *mm*)

(a) Drill 14 mm diameter holes for the lohpgngitudinal rebars at the end plate

(b) Weld the steel column and the stiffening box on the end plate

(c) Insert the longitudinal rebars into the holes and weld to the end plate

(d) Repeat the same procedure for the top end of the specimen

Fig. 2 Preparation of column specimen before casting of concrete

## 2. Experimental program

### 2.1 Specimen design and preparation

A total of 10 specimens were tested under concentric compression, eccentric compression, and two-point-load bending, having the effects of parameters such as spacing of stirrups, dosage of steel fibres and load eccentricity being investigated. The specimen details are shown in Table 1. The encased steel columns were in hot-rolled H section and the concrete cover thickness to the steel column was 50 mm, this satisfied the minimum requirement of Eurocode 4 (EN 1994-1-1 2004) to which the steel contribution ratio also conformed. Considering the maximum spacing (i.e., 150 mm) (EN 1992-1-1 2004) and the limits of reinforcement ratio (i.e., 0.3% ≤ As/A ≤ 6%) (EN 1994-1-1 2004), 8 nos. longitudinal rebars with a diameter of 12 mm were used. Steel rebars with a diameter of 8 mm were used for the stirrups. The cover thickness to the surface of stirrup was 15 mm and 25 mm, respectively, which conformed to the requirements of Eurocode 2 (EN 1992-1-1 2004). The height of all column specimens was 840 mm and the resulted non-dimensional slenderness ratio was 0.16 calculated according to Eurocode 4 (EN 1994-1-1 2004), this is to eliminate the second-order effect as the buckling reduction factor is equal to 1.0. The span of the beam specimen was 2400 mm, this ensured that the flexural failure in the pure bending moment zone would come earlier than the shear failure near the supports, according to a preliminary calculation on the shear and bending moment resistance of the beam. The fabrication details of the specimens are shown in Fig. 1.

The preparation of column specimens before concrete casting is illustrated in Fig. 2. To make sure the longitudinal rebars are transferring bending moment in tension zone under the eccentric load, they were welded into the pre-drilled holes with full-penetration plug welds at both ends. The stiffening boxes were welded to the end plates to prevent the pre-mature concrete crush near the ends and for the positioning of rebars, steel column and formwork. The concrete was cast with the specimens horizontally laid on the ground, and the vibration poker was used during casting. The specimens were covered with the plastic sheets and cured in lab air. For the beam specimen, there were no end plates and stiffening boxes as it was simply supported during the test. It was prepared similarly to the conventional reinforced concrete (RC) beam.

### 2.2 Material properties

The mix proportions of UHSC are given in Table 2. The coarse aggregates were made from basalt gravels with a particle size range of 5~10 *mm* and 10~20 *mm* mixed in a ratio of 4:6, the apparent density was 2850 $kg/m^3$. The fine aggregates were the medium-coarse river sands with a fineness modulus of 2.82. Six standard cubes with a size of

Table 2 Mix proportions of concrete (unit: $kg/m^3$)

| W/B | Cement ($kg/m^3$) | Silica fume ($kg/m^3$) | Water ($kg/m^3$) | Sand | Coarse aggregate ($kg/m^3$) | Superplasticizer ($kg/m^3$) | Specimen group |
|---|---|---|---|---|---|---|---|
| 0.18 | 810 | 90 | 162 | 588 | 882 | 18 | A |
| 0.15 | 821 | 91 | 137 | 593 | 890 | 18 | B~D |

*Note: W/B is the water-binder ratio

without fibers fiber dosage = 0.5% fiber dosage = 1% fiber dosage = 1.5%

Fig. 3 Failure modes of concrete with different dosages of steel fibres

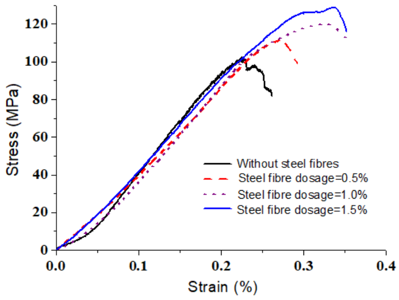


Fig. 4 Stress-strain curves of concrete with different dosages of steel fibre

100 mm × 100 mm × 100 mm were prepared for material tests, they were cured in lab air after casting for 24 hours and then in the fog room with a humidity of 98% for 28 days. The compressive strength and elastic modulus of UHSC used in the CES specimens are given in Table 1.

Addition of steel fibres is expected to further improve the strength of UHSC, however, it would deteriorate the ductility of the UHSC as well as the workability during casting. To determine the proper dosage of steel fibers used in the CES specimens, the effect of steel fibres on the mechanical properties of the UHSC was investigated separately. The circular-shape steel fibres with a diameter of 230 $\mu m$ and a length of 14 $mm$ were used. The failure modes and stress-strain curves of UHSC with different dosages of steel fibres are shown in Figs. 3 and 4. The concrete without steel fibers crushed into pieces and showed very brittle behaviour, as the dosage of steel fibers increased, the failure became more ductile. In Fig. 4, the addition of steel fibres improved the compressive strength and peak strain but had little influence on the compressive stiffness in terms of the initial slope of the stress-strain curve. The effect was significant when the dosage of steel fibres was less than 1.0% in volume, but insignificant when the dosage further increased. Besides, the addition of 1.0% steel fibres was found to have seriously affected the workability of UHSC during casting in this study, previous studies also revealed this (Xiong and Liew 2015). In these regards, the dosage of steel fibres not higher than 0.5% was adopted to prepare the CES specimens shown in Table 1.

Three coupons were respectively cut from the flanges and webs of the encased steel section for the standard tensile tests conforming to ASTM E 8M/E8M-16 (2016). Three coupons were also prepared for each longitudinal rebar and stirrup which are graded as HRB500 according to Chinese code GB 50010 (2010). The basic material properties of the steels are given in Table 3. It can be found that the yield strength of coupon from the web was higher than that from the flange, but the elastic moduli were quite close. Besides, the longitudinal rebars had higher yield strength but comparable elastic modulus with the stirrups.

### *2.3 Test setup and instrumentation*

Fig. 5 shows the layout of strain gauges (SGs) and linear variable differential transformers (LVDTs) for the column specimens. All SGs were unidirectional, placed at mid-height of the column and along with the directions in which the material was stretched or compressed. The strain gauges were wrapped with plastic tapes to prevent damages during

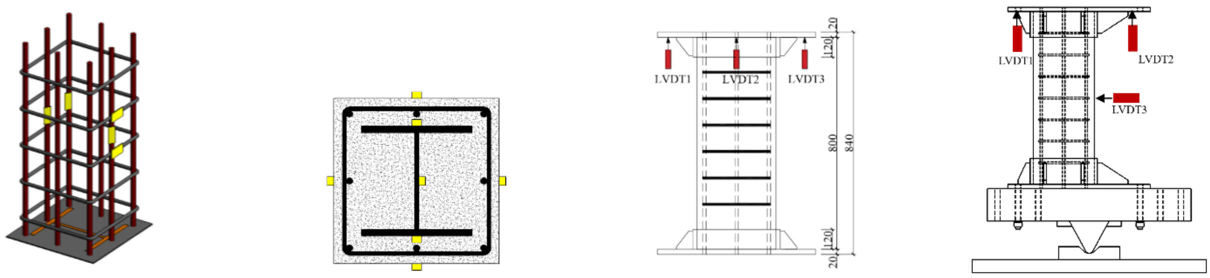


(a) Strain gauges on longitudinal rebars and stirrups (b) Strain gauges on surfaces of concrete and steel section (c) LVDTs for specimens without load eccentricity (d) LVDTs on for specimens with load eccentricity

Fig. 5 Instrumentation for column specimens

Table 3 Mechanical properties and steel reinforcements and steel section

| Series | Cross-section diameter/shape (*mm*) | Yield strength, fy (MPa) | Young modulus (GPa) |
|---|---|---|---|
| Longitudinal rebars | D12 | 533.9 | 192.2 |
| Steel stirrups | D8 | 489.8 | 194.2 |
| Encased section (flanges) | H 200×200×8×12 | 374.6 | 205.7 |
| Encased section (webs) | | 384.5 | 203.0 |

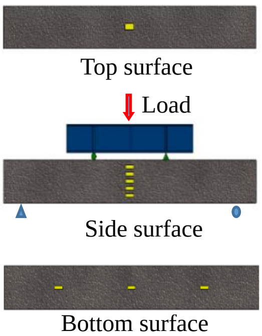


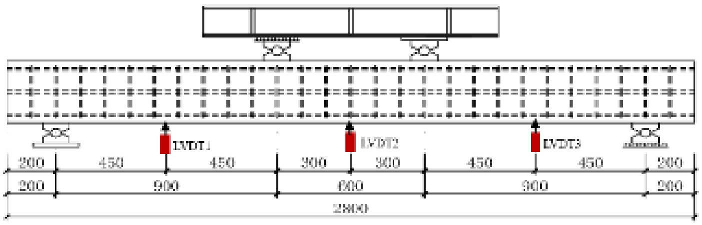


(b) Layout of LVDTs (unit: *mm*)

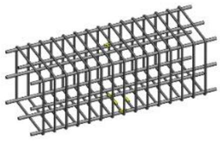

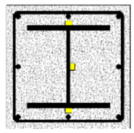

(a) Strain gauges on beam surfaces (c) Strain gauges on longitudinal rebars and stirrups (d) Strain gauges on surfaces of steel section

Fig. 6 Instrumentation for beam specimen

(a) Concentric compression

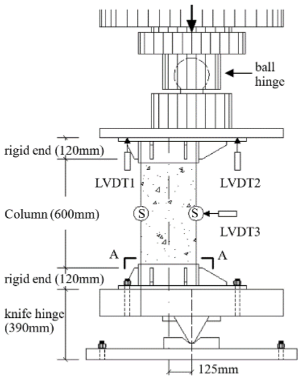


(b) Eccentric compression


(c) Two-point-load bending

Fig. 7 Test setups

concrete casting. The instrumentation for the beam specimen is shown in Fig. 6. Considering the bending moment diagram, the unidirectional SGs on the longitudinal rebars were placed at mid-span of the beam. The SGs on the encased steel section was also placed at mid-span.

Fig. 7 shows the test setups. For compression tests without load eccentricity, a pre-load abou 1000 *k*N was applied to check the alignment between the loading head and the column specimen by observing the readings of SGs and LVDTs. After unloading, it was then reloaded with a rate of 1.0 *mm/min* until it failed. For the compression tests with the load eccentricity, the specimen was pre-loaded to 1000 *k*N and then fully unloaded, after that, it was loaded up to 80% of its peak at a deflection rate of 0.5 *mm/min*, and then loaded to fail at a rate of 0.2 *mm/min*. It should be mentioned that a V-shaped support was used at the bottom and aligned with a ball support at the top (not shown in Fig. 6(b)) to apply the eccentric load. For the bending test, a pre-load up to 80 *k*N was applied. After unloading, the specimen was reloaded to fail at a rate of 0.5 *mm/min*.

## 3. Test results and discussions

### *3.1 Test observations and failure modes*

Fig. 8 shows the failure modes of axially loaded specimens without steel fibres in group A. According to the test observations, there was generally no cracks on surfaces of the specimens when the loads slowly went up to 80% of their peaks. After that, as the load increased, the axial strain increased faster per unit load, indicating plastic deformation


(a) GJ-1 ($s$ = 100 *mm*, $c$ = 25 *mm*) (b) GJ-2 ($s$ = 100 *mm*, $c$ = 15 *mm*) (c) GJ-3 ($s$ = 75 *mm*, $c$ = 15 *mm*) (d) GJ-4 ($s$ = 50 *mm*, $c$ = 15 *mm*)

Fig. 8 Failure modes of specimens without steel fibres under concentric compression

(a) GJ-5 (SF 0.3%, $s$ = 50 *mm*) (b) GJ-6 (SF 0.4%, $s$ = 50 *mm*) (c) GJ-7 (SF 0.5%, $s$ = 50 *mm*)

Fig. 9 Failure modes of specimens with steel fibres under concentric compression

occurred. At the onset of the peak load, a loud sound could be clearly heard, and the longitudinal rebars buckled as the cover concrete spalled (see GJ-1 and GJ-2). Possibly the specimen with a larger cover thickness (i.e., GJ-1) failed in shear with a shear plane seen, which accorded with the concrete fracture pattern Type 4 defined in ASTM C39 (2018). For the specimen with a smaller cover thickness (i.e., GJ-2), it failed with well-formed cones on ends, falling in fracture pattern Type 1 in ASTM C39. However, for the specimen with a further increased spacing of stirrups (i.e., GJ-4), the failure mode of concrete tended to be Type 3 in ASTM C39 where columnar vertical cracks occurred with no well-formed cones.

Fig. 9 shows the failure modes of the axially loaded specimens having different dosages of steel fibres. According to the observations during testing, the cracks on concrete surfaces generally occurred until the axial loads reached 80% ~ 95% of their peaks, which was later than the un-reinforced specimens in Group A. Failure sound can still be heard at onset of peak load but it deteriorated with the increase of fibre dosage, indicating the beneficial effect of steel fibres to improve the ductility after the peak load. The failure mode of concrete seemed not to be changed with various steel fibre dosage as the concrete fractured generally in pattern Type 3 according to ASTM C39 (2018) where the vertical cracks were formed.

Fig. 10 shows the failure modes of the eccentrically loaded specimens with steel fibres. For the specimen with a load eccentricity of 35 *mm* (i.e., GJ-8), small horizontal cracks on the compression side can be found when the load reached 80% of its peak according to the test observation. The cracks were then enlarged and propagated when the load further went up to 95% of its peak, then the concrete cover on the compression side suddenly bulged and spalled in a small extent when the peak load was reached. The horizontal cracks were however not found on the tension side at peak load, indicating there might be no tensile stresses on the tension side due to the counterbalance of compression stresses from the axial load, or the tensile stresses were smaller than the tensile strength of concrete. Nevertheless, the horizontal cracks on the tension side

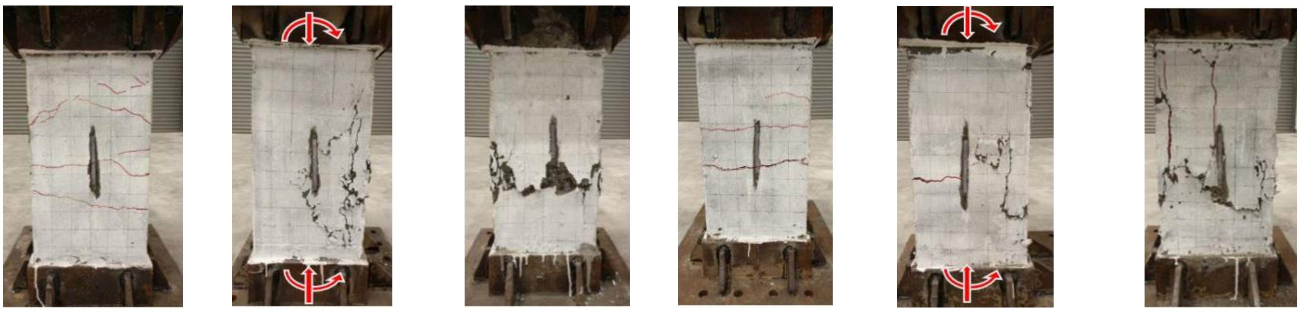

tension side bending direction compression side tension side bending direction compression side

(a) GJ-8 with 35 *mm* eccentricity (b) GJ-9 with 125 *mm* eccentricity

Fig. 10 Failure modes of specimens with steel fibres under eccentric compression

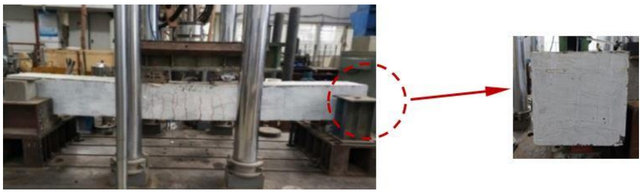

(a) CES beam under bending at failure

(b) No extrusion of encased steel section from ends of the beam

Fig. 11 Failure mode of beam specimen subject to two-point loads under bending

finally occurred in the descending stage of the load. For the specimen with a load eccentricity of 125 mm (i.e., GJ-9), the horizontal cracks occurred on the tension side when the load reached 90% of its peak. Both horizontal and vertical cracks appeared on the compression side. When the load went to its peak, the concrete crushed and the area of crushed concrete was smaller than that of the specimen with smaller load eccentricity (i.e., GJ-8).

Fig. 11 shows the failure mode of the beam specimen under the two-point-load bending. According to the test observations, small vertical cracks occurred in the tension zone at the bottom when the load reached approximately 30% of its peak, then they were retarded due to the hindering of the encased steel section. The vertical cracks slowly propagate upwards to the top flange of the steel section when the load went up to about 80% of its peak, along with the horizontal cracks occurring in the compression zone at the top. As the load further increased, the outward bulges of concrete could be seen in the compression zone to which the vertical cracks also extended. Overall, the CES beam failed in a typical flexural mode like the conventional RC beam where the concrete was crushed in the compression zone at the top and the vertical cracks were produced in the tension zone at the bottom. Besides, it is important to know that there was no extrusion of the encased steel section from the concrete at the ends of the beam where the shear force was the largest (see Fig. 10(b)). This implied that a good interfacial bond was formed between the steel section and concrete so that they could work compatibly to take the shear force and then transfer the bending moment. This is different from the conventional composite beam where shear studs are additionally needed to prevent slip between the steel beam and the concrete slab at the top. The reason is that the steel fibres were added so that the tensile strength of concrete was improved and the concrete cracks were prevented; as a result, the bond strength was improved (Harajli 2010).

### *3.2 Axial load - Deformation relationships*

#### *3.2.1 Concentrically loaded specimens without steel fibres in Group A*

Fig. 12(a) shows that the axial load - vertical displacement curves of the specimens in group A. The specimen GJ-3 had the highest ultimate strength in terms of the peak load and the axial stiffness in terms of the slope in elastic stage, this is because the concrete strength of GJ-3 was the highest. Generally, the smaller the spacing of stirrups was, the higher was the ultimate strength (i.e., GJ-4 vs GJ-2). Besides, it is worth noting that the ultimate strength decreased with the decrease of a cover thickness (i.e., GJ-1 vs GJ-2), in other words, it decreased with the increase of the area of the confined concrete core. This might be due to the fact that the increase of cover thickness reduced the volumetric ratio of stirrups (i.e., the volume of stirrups to the volume of confined concrete core),

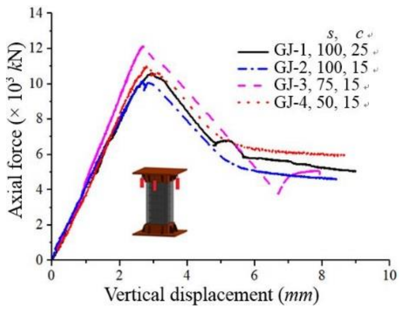


(a) Axial force versus vertical displacement

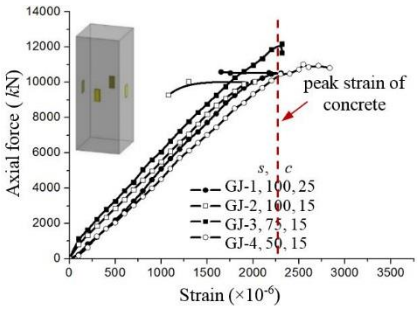


(b) Axial force-strain curves of concrete

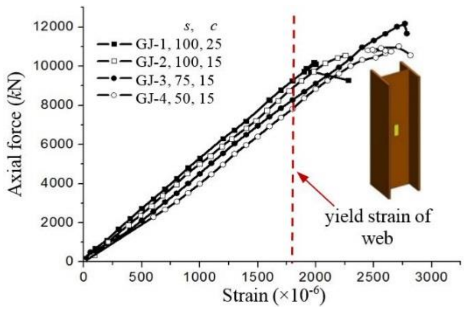


(c) Axial force-strain curves of steel web

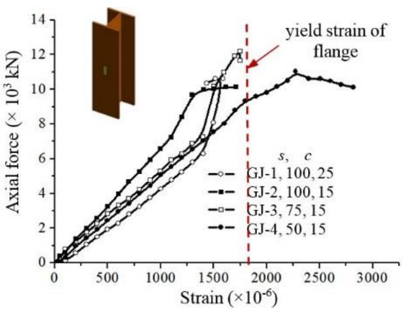


(d) Axial force-strain curves of steel flange

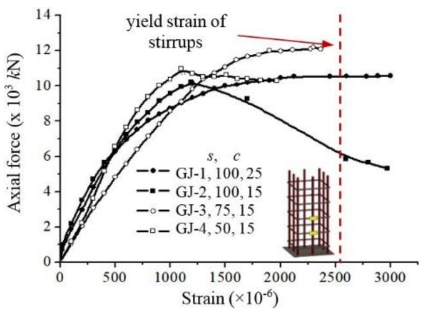


(e) Axial force-strain curves of stirrups

Fig. 12 Axial force-deformation curves of specimens in group A

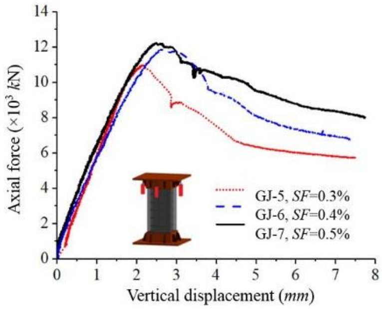


(a) Axial force versus vertical displacement

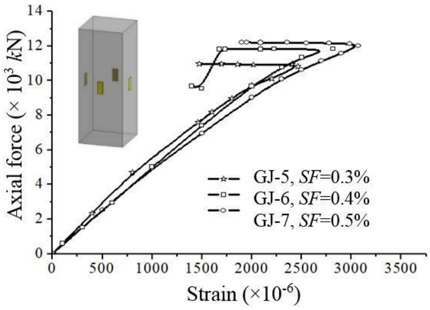


(b) Axial force-strain curves of concrete

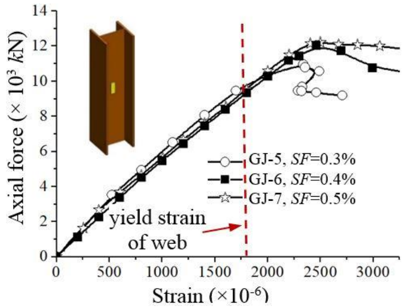


(c) Axial force-strain curves of steel web

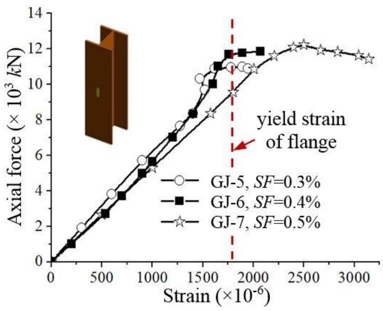


(d) Axial force-strain curves of steel flange

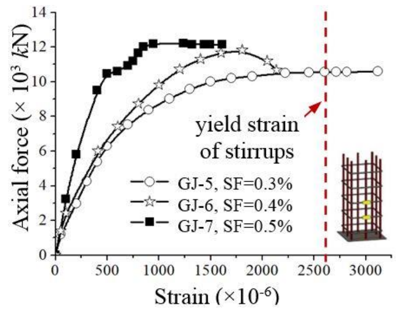


(e) Axial force-strain curves of stirrups

Fig. 13 Axial force-deformation curves of specimens in group B

consequently the confining stress on the concrete was reduced (Mander *et al*. 1988), as a result, the strength of the confined concrete core was lower. Regarding the descending parts, the loads started to drop after their peaks had been reached, and it is believed the drop was due to the crush of concrete. However, the load did not drop to vanish, instead, it dropped into a plateau which might be caused by the yielding of encased steel column ahead of strain hardening.

The axial load-strain curves of concrete are given in Fig. 12(b). It is known that the peak strain of plain concrete corresponding to its compressive strength was about 2250 millionths (see Fig. 4). Fig. 12(b) shows that the concrete of specimens GJ-1 and GJ-3 might spall around their peak strains as the readings of the strain gauges terminated around said strains. However, the concrete of specimen GJ-2 spalled before the peak strain, which also explains why its ultimate strength was the lowest according to Fig. 12(a). For the specimen GJ-4, the concrete spalled after the peak strain had been reached, indicating a better ductility gained by improving the spacing of stirrups to prevent such spalling. Overall, the axial load-strain curves of concrete demonstrated that increasing the cover thickness or reducing the spacing of stirrups could effectively prevent premature spalling of the UHSC. It should be mentioned that the premature spalling could also occur for CES columns with NSC, to account for this, a reduction factor of 0.85 is recommended in Eurocode 4 to reduce the concrete strength (Johnson and Anderson 2004).

The stress-strain curves of the web and flanges of the encased steel column are shown in Figs. 12(c) and (d), respectively. Average readings from strain gauges were plotted for each column. According to Eurocode 3 (EN 1993-1-1 2005), the flanges fall in Class 1 whereas the web can be classified into Class 2. For Class 1 sections, the local buckling would not occur in the plastic range where it would appear for Class 2 sections. This is the reason why the post-yield strains on the web could be measured (see Fig. 12(c)) whereas they nearly could not be measured on the flanges (see Fig. 12(d)) as the strain gauges were spoiled by the local buckling except for GJ-4 with a spacing of stirrups of 50 mm. This indicates increasing the spacing of stirrups is beneficial to fully make use of the strength of steel.

Fig. 12(e) shows the axial load-strain curves of the stirrups. For the specimens GJ-1 and GJ-3, there were no load drops but the strains of the stirrups experienced large development. This might be because the strain gauges on the stirrups were disturbed by sudden spalling of concrete or yielding of longitudinal rebars so that they produced a large strain in a small increment of load. Possibly the stirrups had not yielded before the peak loads were achieved as the turning points of the curves were ahead of the yielding points of steel. For the specimens GJ-2 and GJ-4, it is clearly seen that the stirrups had not yielded before the load peaks, thus the strength of the stirrups was not fully utilized. It may be reasonable to ignore the confinement from the stirrups as done by the Eurocode 4 (EN 1994-1-1 2004).

### *3.2.2 Concentrically loaded specimens with steel fibres in Group B*

The axial load versus vertical displacement curves of the specimens in Group B are shown in Fig. 13(a). The stiffness in the elastic stage was quite similar, indicating the addition of steel fibres had little influence on the elastic stiffness of the CES columns, this accorded with plain concrete as shown in Fig. 4. In general, the ultimate strength of the CES column (i.e., the peak load) increased with the increase of dosage of the steel fibres, and it was improved more when

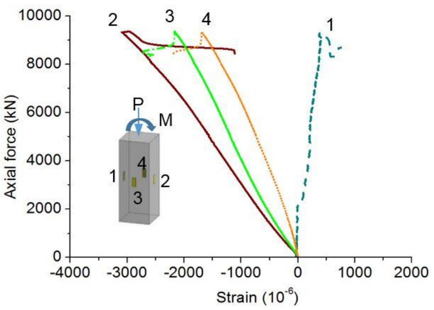


(a) Load-strain curves of concrete of GJ-8

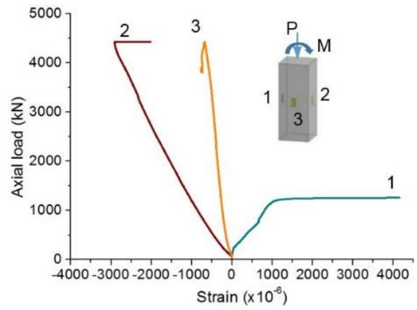


(b) Load-strain curves of concrete of GJ-9

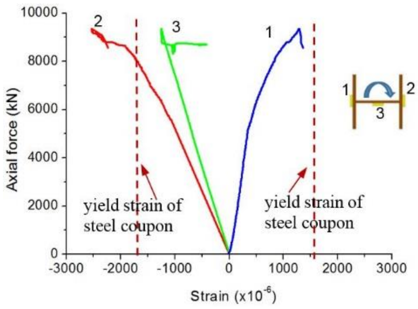


(c) Load-strain curves of H steel of GJ-8

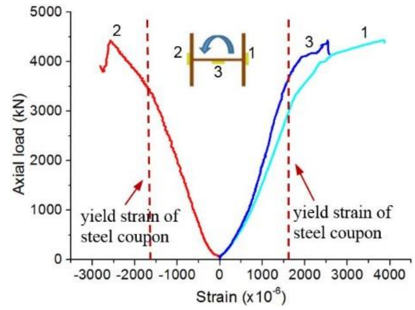


(d) Load-strain curves of H steel of GJ-9

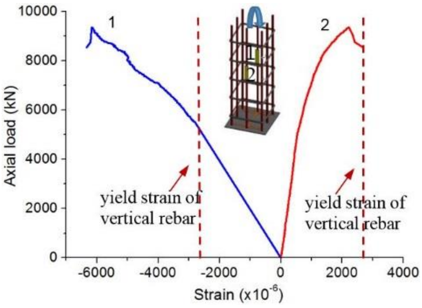


(e) Load-strain curves of rebars of GJ-8

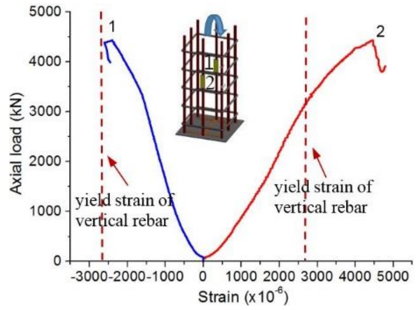


(f) Load-strain curves of rebars of GJ-9

Fig. 14 Axial force-deformation curves of specimens under eccentric load

the fibre dosage increased from 0.3% to 0.4% than was the case from 0.4% to 0.5%. Fig. 4 also showed the same phenomenon where the strength of concrete was improved more when the fibre dosage increased from 0.5 % to 1.0% than was the case from 1.0% to 1.5%. Besides, the specimen GJ-7 with an addition of 0.5% steel fibres showed the best ductility in terms of the load dropping rate after the peak load had been reached.

Fig. 13(b) shows the axial load - longitudinal strain curves of concrete. The descending parts were not measured, this was due to the crush of concrete that terminated the readings of strain gauges. The strain at termination increased with the increase of steel fibre dosage.

The axial load versus longitudinal strain curves of steel web and flanges are given in Figs. 13(c) and (d), respectively. Obviously, the steel web and flanges had yielded before the peak loads were reached. Also, the post-yield strains of the web could be better captured by the strain gauges than was the case for the flanges due to the Class 2 classification, indicating the encased steel columns can be fully utilized even the concrete strength was increased by the steel fibres.

The relationship between the axial load and the longitudinal strain of the stirrups are shown in Fig. 13(e). Similar to the specimens in Group A un-reinforced by the steel fibres, the peaks load of the columns came earlier than the yielding of the stirrups. Besides, it is worth noting that the peak strain of stirrup corresponding to the peak load was in an inverse proportion to the fibre dosage. The higher the dosage was, the smaller was the peak strain. This might be because the strength of concrete was improved by the steel fibres, but the lateral deformation of which was reduced.

### *3.2.3 Eccentrically loaded specimens with steel fibres in Group C*

The specimens were loaded with bending about the major axis of the encased steel section. Figs. 14(a) and (b) shows the load-strain curves of concrete of the specimen GJ-8 and GJ-9, respectively. The concrete of both specimens at the far side of the eccentric load was subject to tensile stress. For the concrete at the near side of the eccentric load, they failed at different compression strains. Basically, the higher the load eccentricity was, the smaller was the failure compression strain. This implied that at least the concrete of specimen GJ-9 at the near side of the eccentric load was not fully utilized. For the specimen GJ-8, it is not sure if said concrete was fully utilized as the peak compression strain of standard concrete cylinder corresponding to its compressive strength was not captured. However, it is noted that the concrete strength of specimen GJ-8 is quite close to that of concrete with an addition of 1.5% steel fibres shown in Fig. 4. If the peak strain of concrete with 1.5% steel fibres (i.e., 3385 millionths) is referred to and compared with the failure compression strain of specimen GJ-8 (i.e., 3098 millionths), it could be concluded that said concrete of GJ-8 was also not fully utilized. For the parts of concrete near the neutral axis, it is clearly seen they were not fully utilized according to the strains measured by the strain gauges No.3 and No.4. Considering this, the plastic design could not be adopted. Alternatively, a proper reduction factor may be introduced like the Eurocode 4 (EN 1994-1-1 2004), this will be discussed in Section 4.

The load-strain curves of the steel web and flanges are given in Figs. 14(c) and (d). For the specimen with a smaller load eccentricity (i.e., GJ-8), the steel flange at the near side of eccentric load yielded in compression, but the web and the flange at the far side of the eccentric load did not yield. The web was under compression, indicating the neutral axis lied close to the flange in tension. For the specimen with a greater load eccentricity (i.e., GJ-9), all flanges and web had yielded before the peak load was achieved. The strains of web and the flange at the far side of the eccentric load were quite close, indicating the normal stress distribution between the centre of the web and the flange in tension almost approached rectangular stress block, and the neutral axis lied close to the flange in compression.

Figs. 14(e) and (f) give the load-strain curves of the longitudinal rebars. For the specimen GJ-8, the longitudinal rebars yielded in compression but the ones at the far side of the eccentric load did not yield in tension, which is similar to the flange of the encased steel section. However, for the specimen GJ-9, the rebars in compression did not yield unlike the flange of the encased steel section in compression (see Fig. 14(d)), this was attributed to the fact that the yield strain of the rebars is quite larger than that of the encased steel section.

### *3.2.4 Laterally loaded specimen with steel fibres in Group D*

The bending moment-displacement curves of the CES beam specimen GJ-10 subject to a two-point-load bending are given in Fig. 15(a). The bending moment in the pure moment zone (i.e., the part of the beam between the two-point loads) was used. It is seen that the curves from LVDT1 and LVDT3 were rather close, implying they were symmetrically positioned meanwhile the specimen was symmetrically loaded on the two loading points. There were load drops after the peak load had been achieved due to the crush of concrete in the compression zone. After the drops, the load was sustained with the increase of vertical displacement. It is believed that the load was taken and sustained by the partially-encased beam comprised of the steel section and the concrete inside it. It is of much interest to know if there would be another load drop caused by the concrete crush inside the steel section, in which case the load is taken by the pure steel section. This could be investigated in future study.

The bending moment-strain curves of the concrete along the height of the CES beam are shown in Fig. 15(b). The spacing of the strain gauges was 50 *mm*. The readings of strain gauge No. 2 was not captured due to its spoiling. The strain gauge No. 5 was subject to tension and the others were subject to compression, indicating the neutral axis approached the bottom surface of the beam, and this is

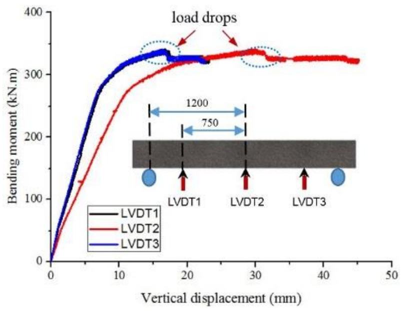


(a) Load-vertical displacement curves

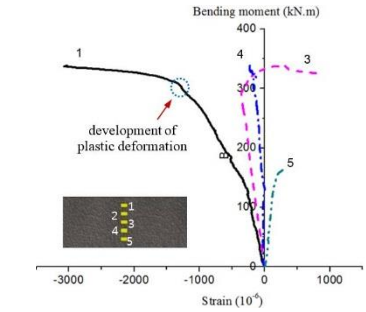


(b) Load-strain curves of concrete

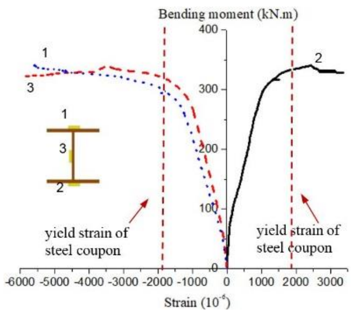


(c) Load-strain curves of encased steel beam

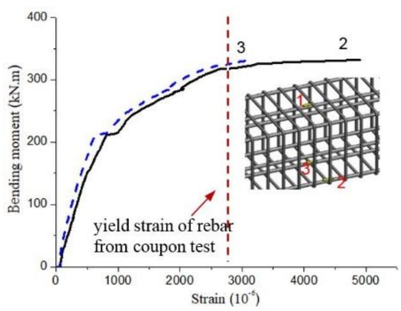


(d) Load-strain curves of rebars

Fig. 15 Axial force-deformation curves of the specimen under two-point-load bending similar to the over-reinforced RC beam. In fact, the neutral axis lied in between the strain gauges No. 4 and No. 5 and was close to the strain gauge No. 4. The concrete at strain gauge No. 1 tended to develop plastic deformation around a strain of 1400 millionths which was much smaller than the peak strain of a standard concrete cylinder (see the peak strain of concrete with 1.5% steel fibres in Fig. 4), indicating there might be premature failure of concrete in the compression zone.

Fig. 15(c) shows the bending moment-strain curves of the encased steel beam. Generally, the strain of the flange in compression was smaller than that in tension at a given load level. The strains of the web and flange in compression were close, this was contrary to the case of CES column under a larger load eccentricity (i.e., GJ-9). It also indicated the neutral axis was close to the flange in tension, this had been proved by the concrete strain distribution as mentioned above. The location of the neutral axis also explained why the strain of flange in tension was higher than that in compression at a given load level. Besides, both the flanges and web had yielded before the peak bending moment was achieved. This is important to know that the full plastic moment resistance of the steel beam had been achieved and can be used to determine the moment resistance of the CES beam under bending.

The bending moment-strain curves of the longitudinal rebars are shown in Fig. 15(d). It can be found that the rebars in the tension zone had yielded before the peak bending moment was reached. The strains of the rebars in the compression zone (i.e., strain gauge No. 1) were not captured. However, it is believed they had yielded also as the neutral axis was close to the bottom surface of the beam as mentioned above and if the cross-section remained plane. The force equilibrium on the cross-section was reached by the counterbalance between the material strengths in the tension zone (i.e., the yielded bottom flange and lower part of web of the steel beam, and the yielded rebars at bottom) and the material strengths in the compression zone (i.e., the yielded top flange and upper part of web of the steel beam, the compressed but prematurely failed concrete in compression zone, and the yielded rebars at top).

### *3.3 Ductility*

It is important to evaluate the ductility of the CES members after their peak loads when the UHSC is used. In the present study, a ductility index ($\mu$) as defined by Eq. (1) is used to compare the ductility of various CES specimens

$$\mu = \Delta_{0.85}/\Delta_y \tag{1}$$

where $\Delta_{0.85}$ is a displacement corresponding to a load level after the load has dropped to 85% of its peak load, and $\Delta_y$ is the displacement corresponding to the proportional limit, and taken as the displacement corresponding to a load that is the intersect of a horizontal line from the peak load and a regressed line for the initial straight part of the load-displacement curve. Eq. (1) was used by various researchers to evaluate the ductility of RC columns (Pessiki and Pieroni 1997) and concrete filled tubular columns (Tao *et al*. 2007). The ductility index and ductility ratio of specimens under concentric loads are given in Fig. 16. The ductility indices of specimens GJ-2 and GJ-5 are used as benchmark (i.e., their ductility ratio is 1.0) to determine the ductility ratio of other test specimens. By comparing GJ-2 and GJ-1, the ductility index showed little variation with the increase of cover thickness. But when comparing GJ-4 with GJ-2, the ductility index was improved by reducing the spacing of stirrups. The ductility index of GJ-3 is low due to its higher concrete strength than the other test specimens. The ductility can be enhanced by increasing the dosage of steel fibres according to the specimens with steel fibres in Group B. The increase of ductility index was about 18% for every increment of 0.1% volumetric steel fibre content in the concrete starting for Specimen GJ-5 with 0.3% steel fibre content to Specimen GJ-7 with 0.5% steel fibre content. Besides, it is important to know that the CES columns with the UHSC having a spacing of stirrups of 50 mm and an addition of steel fibres of 0.5% in volume can achieve an equivalent ductility to those with the NSC presented in previous studies (Liu *et al*. 2015).

## 4. Comparisons with code predictions

The axial load versus bending moment interaction curve can be used to determine the axial load capacity, bending moment resistance and beam-column capacity of the CES members. The interaction curve of Eurocode 4 (EN 1994-1-1 2004) is given in Fig. 17 and assumed to be a polygonal diagram. The selected points on the curve are derived based on the plastic analysis. The tensile strength of the concrete is ignored conservatively and a full composite action without slip between the encased steel section and the

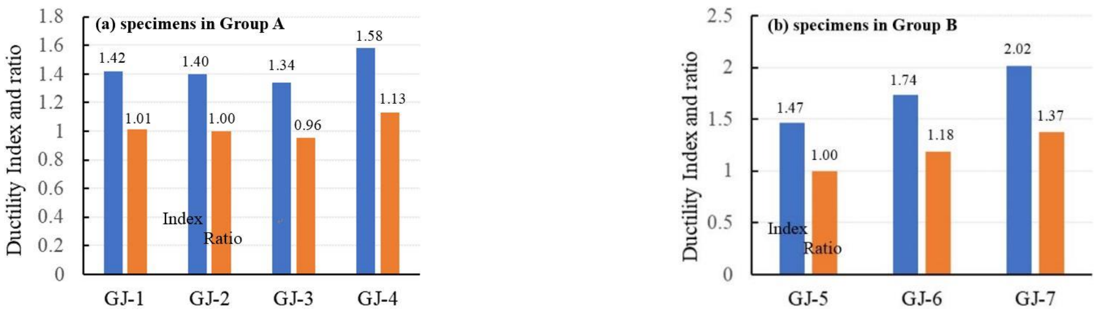


Fig. 16 Ductility indices and ratios of specimens under concentric loads

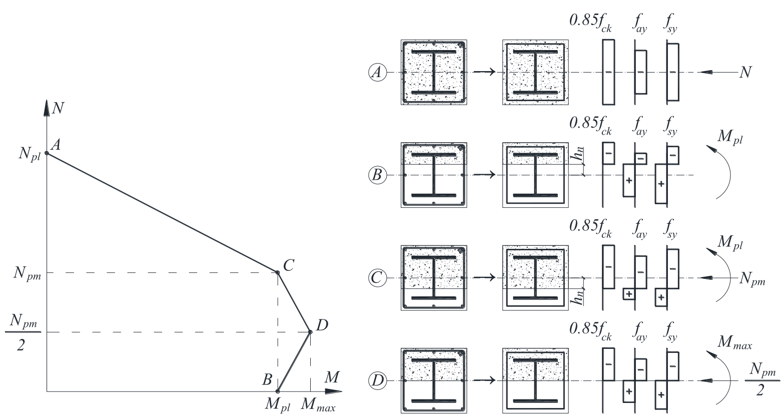


Fig. 17 Resistance interaction curve in Eurocode 4 for CES members

encasing concrete is assumed. The interaction curve is independent on the slenderness of the CES member and only related to its cross-sectional geometries and material strengths. The load capacities corresponding to the selected points on the curve can be calculated according to Eqs. (2)~(5).

$$N_{pl} = A_a f_{ay} + 0.85 A_c f_{ck} + A_s f_{sy} \tag{2}$$

$$N_{pm} = 0.85 A_c f_{ck} \tag{3}$$

$$\begin{aligned} M_{pl} = &\left(W_a - W_{a,n}\right) f_{ay} + 0.5\left(W_c - W_{c,n}\right) f_{ck} \\ &+ \left(W_s - W_{s,n}\right) f_{sy} \end{aligned} \tag{4}$$

$$M_{max} = W_a f_{ay} + 0.5 W_c f_{ck} + W_s f_{sy} \tag{5}$$

where $A_a$, $A_c$, $A_s$ is the cross-sectional area of the encased steel section, concrete and longitudinal rebars, respectively; $E_a$, $E_c$, and $E_s$ is the corresponding elastic modulus and $f_{ay}$, $f_{ck}$, and $f_{sy}$ is the corresponding strength. For simplicity, the longitudinal rebars are equivalently converted into a rectangular tube based on the same cross-sectional area and position of centerline (Liew and Xiong 2015). $W_a$, $W_c$, $W_s$ are the plastic section modulus of the steel section, concrete section, and the longitudinal rebars, respectively; and $W_{a,n}$, $W_{c,n}$, $W_{s,n}$ is the plastic section modulus of the corresponding component within the area of $2h_n$ from the centerline of the composite section where $h_n$ is the depth of the neutral axis from the centerline. $N_{pl}$ is the axial capacity of the short CES columns under concentric axial loads and $M_{pl}$ is the plastic moment resistance of flexural CES beams under bending. The factor 0.85 in Eq. (2) is to consider the premature crushing of unconfined concrete under compression (Johnson and Anderson 2004). To determine the beam-column resistance, the geometric equations for the three segments of the interaction curve should be used and given in Eqs. (6)~(8). The unknown is the maximum axial load $N_u$ that can be taken by the CES column with a given load eccentricity $e_a$.

Segment AC

$$\frac{N_u - N_{pm}}{N_{pl} - N_{pm}} + \frac{k N_u e_a / \alpha_M}{M_{pl}} = 1 \tag{6}$$

Segment CD

$$\frac{N_u - 0.5 N_{pm}}{0.5 N_{pm}} + \frac{k N_u e_a / \alpha_M - M_{pl}}{Mpl_{max}} \tag{7}$$

Segment DB

$$\frac{N_u}{0.5 N_{pm}} + \frac{k N_u e_a / \alpha_M - M_{max}}{M_{pl,Rk} - M_{max} = 1} \tag{8}$$

where $k$ is an amplification factor considering the second-order effect due to the load eccentricity and calculated in Eq. (12) and for short column, $k$ is 1.0 ; $\beta$ is an equivalent moment factor taken as 1.1 for bending moments from the eccentric axial load (EN 1994-1-1 2004), the member bow imperfection was ignored as it was rather smaller than the load eccentricity; $N_{cr,eff}$ is the Euler's buckling load. As the axial load $N_u$ is much smaller than the Euler's buckling load, the amplification factor $k$ was approximately taken equal to the equivalent moment factor $\beta$ in the present study. It should be mentioned that, although the steel with nominal yield strength up to 460 N/mm$^2$ is allowed by Eurocode 4, there has been researches (Liu *et al*. 2015, Morino 2002, Wakabayashi and Minami 1990, Hegger and Döinghaus 2002 and Hoffmeister *et al*. 2002) on the use of structural steels with yield strengths exceeding 355 N/mm$^2$, finding that the design rules need to be modified for the use with steel grades higher than S355 in order to avoid premature crushing of concrete or partial yielding of steel (Johnson and Anderson 2004). In this regard, the factor $\alpha_M$ is recommended to reduce the moment resistance that is based on the rectangular stress blocks. In Eurocode 4, it is taken as 0.9 for steel grades between S235 and S355 inclusive, and 0.8 for steel grades S420 and S460. In the present study, it was respectively taken as 1.0 and 0.9 for discussion.

$$k = \frac{\beta}{1 - \frac{N_u}{N_{cr,eff}}} \approx \beta \tag{9}$$

The comparisons between the test and predicted resistance are shown in Table 4. The predictions were based on the cylinder strength of concrete which was converted

Table 4 Comparison between test results and code predictions

| Specimen ID | Test load capacity ($N_t$, *k*N) | Predicted by EC4 ($N_a$, *k*N) | Predicted/Test ($N_a/N_t$) |
|---|---|---|---|
| **GJ-1** | 10602 | 10248 | 0.967 |
| **GJ-2** | 10196 | 10135 | 0.994 |
| **GJ-3** | 12186 | 11021 | 0.904 |
| **GJ-4** | 11020 | 10325 | 0.937 |
| **GJ-5** | 10975 | 11843 | 1.079 |
| **GJ-6** | 11841 | 12082 | 1.020 |
| **GJ-7** | 12221 | 12461 | 1.020 |
| **GJ-8** | 9367 | 9004 (9426) | 0.961 (1.006) |
| **GJ-9** | 4437 | 3610 (4260) | 0.814 (0.960) |
| | **Test moment resistance ($M_t$, *k*N·*m*)** | **Predicted by EC4 ($M_a$, *k*N·*m*)** | **Predicted/Test ($M_a/M_t$)** |
| **GJ-10** | 331 | 325 (361) | 0.982 (1.091) |

*Average & standard deviation for predicted/test values = 0.968 & 0.073

from the cubic strength with a conversion factor of 1.0 recommended by Graybeal and Davis (2008). The average and standard deviation of the predicted/test values (values in parentheses are not considered) are 0.968 and 0.073 respectively, showing reasonable agreement between them. Specifically, the predictions for the columns not reinforced by the steel fibres (i.e., GJ-1 ~ GJ-4) were slightly lower than the test values; but for the ones reinforced by the steel fibres (i.e., GJ-5 ~ GJ-7), the predictions were slightly higher. Nevertheless, the predictions are close to the test values for the concentrically loaded columns, indicating the reduction factor 0.85 in Eq. (2) is still applicable to the CES columns with the UHSC. The test axial load capacities of the concentrically loaded columns (i.e., GJ-1~GJ-7) are also shown in Fig. 18 for a better illustration.

Table 4 also shows that the prediction was quite close to the test value for the column with a smaller load eccentricity (i.e., GJ-8) when the reduction factor $\alpha_M$ was either taken as 1.0 or 0.9 (the difference of predictions with different $\alpha_M$ values is 4.7%), indicating a minor influence of it on the beam-column resistance of the CES columns with the small load eccentricities. This is because said resistance was mainly dominated by axial force. For the column with a larger load eccentricity (i.e., GJ-9), the prediction was however quite different from the test value when the reduction factor $\alpha_M$ was taken as different values (the difference of predictions with different $\alpha_M$ values is 17.9%). This is because the beam-column resistance of the CES columns with large load eccentricities was mainly dominated by the bending moment to which the reduction factor $\alpha_M$ was applied. This has also been proved by the beam specimen (i.e., GJ-10) when the predictions and test values were compared with respect to different $\alpha_M$ values (the difference of predictions with different $\alpha_M$ values is 11.1%). Besides, it is worth noting that there was the premature crushing of concrete in the specimens GJ-8 ~ GJ-10 and partial yielding of steel in the specimen GJ-8 according to the test observations and load-strain curves, which could cause loss of resistance. However, the predictions of them were quite close to the test values, this implies that the reduction factors of 0.85 in Eq. (2) and $\alpha_M$ could properly consider the loss of plastic resistance in design.

There is another way to determine the interactive strength of the columns subject to eccentric loads, by using the second-order lateral displacement directly taken from the test measurement instead of using Eq.(12). Fig. 18 shows the test and predicted *M-N* curves for the specimens GJ-8 and GJ-9. The test bending moment were calculated from the test axial load multiplied by the sum of measured

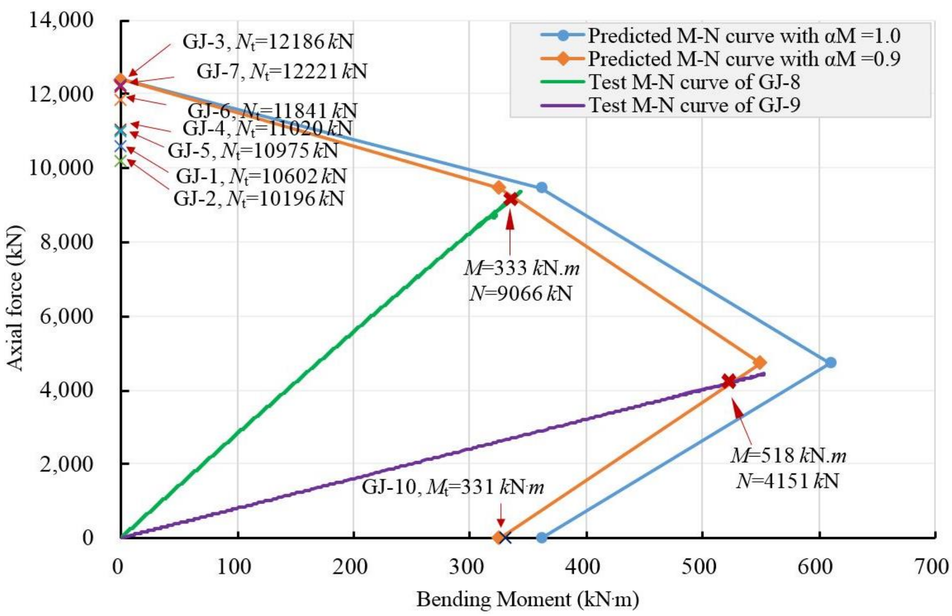


Fig. 18 Test and predicted *M-N* curves for GJ-8 and GJ-9

lateral displacement (i.e., the reading of LVDT 3 shown in Fig. 5) and the load eccentricity. The intersection between the test and predicted M-N curves determines the interactive strength of the column subject to eccentric load. It can be found that the axial load capacities are greater than those given in Table 4 (i.e., those with the reduction factor $\alpha_M$ taken as 0.9). The difference is larger for the column with a higher load eccentricity (i.e., GJ-9). This is because the theoretical second-order lateral displacements based on Eq. (12) are larger than the measured ones in tests, and the difference between the theoretical and measured lateral displacements is larger for the column with a higher load eccentricity. Besides, it is worth noting that the test *M-N* curves cannot reach the predicted one with $\alpha_M$ equal to 1.0, again indicating the $\alpha_M$ value should be taken as 0.9 for the CES members with high strength concrete investigated in this study.

Basically, above comparison between the code-predictions and test results has established the validity of the Eurocode 4 approach for designing CES members with the UHSC. This accorded with the conclusion done by Lai *et al*. (2019), but disagreed with that given by Kim *et al*. (2012 and 2014). This may be due to the fact that, in Kim *et al*.'s research, the material compatibility between the high strength steel (800 MPa) and UHSC (184 MPa) was not achieved, as a result, the steel strength was not fully utilized. In this regard, a further reduction factor besides the code-specified reduction factors may be needed to consider the effect of high strength steel. The high strength steel was not used by Lai *et al*. (2019) and this study.

## 5. Conclusions

The paper investigated the mechanical properties of steel fibre-reinforced UHSC and their effects on concrete encased steel composite columns under compression, combined compression and bending and pure bending. The following conclusions can be drawn for such members made of S355 steel and UHSC with cubic compressive strength up to 140 MPa.

- The failure mode under concentric compression is dependent on the cover thickness of concrete and dosage of steel fibres. The failure mode of fibre reinforced ultra-high strength concrete encased steel columns under eccentric compression is similar to the normal strength CES columns. For column with smaller eccentricity, the first cracks occur at the compression side, whereas for column with larger eccentricity the first cracks occur at the tension side. For steel beam encased with the steel fibre-reinforced UHSC, the test results show good bond capacity at the interface of concrete and steel as no end slip and no interface crack was observed between the steel section and concrete at the beam ends.
- Brittle failure of UHSC is found for CES members subject to eccentricity load. The concrete encased steel section could not develop its fully plastic resistance when the load eccentricity is high.
- The ductility of UHSC can be improved by either reducing the spacing of stirrups or increasing the dosage of steel fibres. The CES columns with the UHSC having a spacing of stirrups of 50 mm and an addition of steel fibres of 0.5% in volume can achieve an equivalent ductility to those with the NSC, and the plastic design method in EC4 can be used to predict the resistance.
- The resistance predicted based on Eurocode 4 is close to the test values, except that Eurocode 4 tends to give a very conservative prediction of the ultimate resistance for the column with a large load eccentricity. This is because the second-order moment predicted by Eurocode 4 assumed a very large equivalent out-of-straightness. Overall, the code-specified reduction factors applied to the concrete strength and moment resistance are capable to consider the loss of resistance due to the premature spalling/crushing of concrete cover and partial yielding of encased steel section.

## Acknowledgments

The authors would like to acknowledge the financial support by the National Natural Science Foundation of China [No. 51878348], and the Guangdong Natural Science Foundation under project [No. 2018A030313752].

## References

ACI 318-08 (2008), Building code requirements for structural concrete and commentary. American Concrete Institute: Farmington Hills, MI, USA.

AIJ (2001), Standard for structural calculation of steel reinforced concrete structures, 5th Ed., Architectural Institute of Japan, Tokyo, Japan.

Begum, M., Driver, R.G. and Elwi, A.E. (2013), "Behaviour of partially encased composite columns with high strength concrete", *Eng. Struct*., **56**, 1718-1727. https://doi.org/10.1016/j.engstruct.2013.07.040

ANSI/AISC 360 (2016), Specification for Structural Steel Buildings, American Institute of Steel Construction, Chicago, IL, USA.

ASTM C39/C39M (2018), Standard test method for compressive strength of cylindrical concrete specimens. ASTM International, West Conshohocken, PA, USA.

ASTM E 8M/E8M (2016), Standard test methods for tension testing of metallic materials, ASTM International, West Conshohocken, PA, USA.

Choi, E.G., Kim, H.S. and Shin, Y.S. (2012), "Performance of fire damaged steel reinforced high strength concrete (SRHSC) columns", *Steel Compos. Struct., Int. J.*, **13**(6), 521-537. https://doi.org/10.12989/scs.2012.13.6.521

El-Tawil, S. and Deierlein, G.G. (1999), "Strength and ductility of concrete encased composite columns", *J. Struct. Eng.*, **125**(9), 1009-1019. https://doi.org/10.1061/(ASCE)0733-9445(1999)125:9(1009)

Ellobody, E. and Young, B. (2011), "Numerical simulation of concrete encased steel composite columns", *J. Constr. Steel Res.*, **67**, 211-222. https://doi.org/10.1016/j.jcsr.2010.08.003

EN 1992-1-1 (2004), Eurocode 2: Design of concrete structures – Part 1-1: General rules and rules for buildings, European

Committee for Standardization.
EN 1993-1-1 (2005), Eurocode 3: Design of steel structures – Part 1-1: General rules and rules for buildings, European Committee for Standardization.
EN 1994-1-1 (2004), Eurocode 4: Design of composite steel and concrete structures – Part 1-1: General rules and rules for buildings, European Committee for Standardization.
Gao, D.Y., You, P.B., Zhang, L.J. and Yan, H.H. (2018), "Seismic behavior of SFRC shear wall with CFST columns", *Steel Compos. Struct., Int. J.*, **28**(5), 527-539. https://doi.org/10.12989/scs.2018.28.5.527
GB 50010 (2010), Code for Design of Concrete Structures, Ministry of Housing and Urban-Rural Development of the People's Republic of China. [In Chinese]
GB 50936 (2014), Technical Code for Concrete-filled Steel Tubular Structures, Ministry of Housing and Urban-Rural Development of the People's Republic of China. [In Chinese]
Graybeal, B. and Davis, M. (2008), "Cylinder or cube: strength testing of 80 to 200 MPa (11.6 to 29 ksi) ultra-high-performance fibre-reinforced concrete", *ACI Mater J.*, **105**(6), 603-609.
Harajli, M.H. (2010), "Bond behavior in steel fibre-reinforced concrete zones under static and cyclic loading: experimental evaluations and analytical modelling", *J. Mater. Civil Eng.*, **22**(7), 674-686. https://doi.org/10.1061/(ASCE)MT.1943-5533.0000067
Hegger, J. and Döinghaus, P. (2002), "High performance steel and high performance concrete in composite structures", In: J.F. Hajjar, M. Hosain, W.S. Easterling and B.M. Shahrooz (eds), *Composite Construction in Steel and Concrete IV*, American Society of Civil Engineers, New York, USA.
Hoffmeister, B., Sedlacek, G., Müller, C. and Kühn, B. (2002), "High strength materials in composite structures", In: J.F. Hajjar, M. Hosain, W.S. Easterling and B.M. Shahrooz (eds), *Composite Construction in Steel and Concrete IV*, American Society of Civil Engineers, New York, USA.
Johnson, R.P. and Anderson, D. (2004), Designers' guide to EN 1994-1-1 Eurocode 4: Design of composite steel and concrete structures - Part 1.1: General rules and rules for buildings, Thomas Telford Publishing, London, UK.
Kara, I.F. and Dundar, C. (2012), "Prediction of deflection of high strength steel fiber reinforced concrete beams and columns", *Comput. Concrete, Int. J.*, **9**(2), 133-151. https://doi.org/10.12989/cac.2012.9.2.133
Kim, C.S. and Hwang, H.J. (2018), "Numerical investigation on load-carrying capacity of high-strength concrete-encased steel angle columns", *Int. J. Concr. Struct. Mater.*, **12**(1), 1-17. https://doi.org/10.1186/s40069-018-0238-7
Kim, C.S., Park, H.G., Chung, K.S. and Choi, I.R. (2012), "Eccentric axial load testing for concrete-encased steel columns using 800 MPa steel and 100 MPa concrete", *J. Struct. Eng.*, **138**(8), 1019-1031. https://doi.org/10.1061/(ASCE)ST.1943-541X.0000533
Kim, C.S., Park, H.G., Chung, K.S. and Choi, I.R. (2014), "Eccentric axial load capacity of high-strength steel-concrete composite columns of various sectional shapes", *J. Struct. Eng.*, **140**(4), 04013091. https://doi.org/10.1061/(ASCE)ST.1943-541X.0000879
Lai, B.L., Liew, J.Y.R. and Wang, T.Y. (2019), "Buckling behaviour of high strength concrete encased steel composite columns", *J. Constr. Steel Res.*, **154**, 27-42. https://doi.org/10.1016/j.jcsr.2018.11.023
Liew, J.Y.R. and Xiong, M.X. (2015), Design guide for concrete filled tubular members with high strength materials to Eurocode 4 - An extension of Eurocode 4 Method to C90/105 Concrete and S550 Steel. Research Publishing Services, Singapore.
Liu, Y., Guo, Z.X., Xu, P.H. and Jia, L.P. (2015), "Experimental study on axial compression behavior of core steel reinforced concrete columns", *J. Build. Struct.*, **36**(4), 68-74.
Mander, J.B., Priestley, M.J.N. and Park, R. (1988), "Theoretical stress-strain model for confined concrete", *J. Struct. Eng.*, **114**(8), 1804-1826. https://doi.org/10.1061/(ASCE)0733-9445(1988)114:8(1804)
Morino, S. (2002), "Recent developments on concrete-filled steel tube members in Japan", In: J.F. Hajjar, M. Hosain, W.S. Easterling and B.M. Shahrooz (eds), *Composite Construction in Steel and Concrete IV*, American Society of Civil Engineers, New York, USA.
Naito, H., Akiyama, M. and Suzuki, M. (2011), "Ductility evaluation of concrete-encased steel bridge piers subjected to lateral cyclic loading", *J. Bridge Eng.*, **16**(1), 72-81. https://doi.org/10.1061/(ASCE)BE.1943-5592.0000120
Pessiki, S. and Pieroni, A. (1997), "Axial load behavior of large-scale spirally-reinforced high-strength concrete columns", *ACI Struct. J.*, **94**, 304-314.
Pons, D., Espinós, A., Albero, V. and Romero M.L. (2018), "Numerical study on axially loaded ultra-high strength concrete-filled dual steel columns", *Steel Compos. Struct., Int. J.*, **26**(6), 705-717. https://doi.org/10.12989/scs.2018.26.6.705
Ricles, J.M. and Paboojian, S.D. (1994), "Seismic performance of steel-encased composite columns", *J. Struct. Eng.*, **120**(8), 2474-2494. https://doi.org/10.1061/(ASCE)0733-9445(1994)120:8(2474)
Sharmila, P. and Dhinakaran, G. (2015), "Strength and durability of ultra fine slag based high strength concrete", *Struct. Eng. Mech., Int. J.*, **55**(3), 675-686. https://doi.org/10.12989/sem.2015.55.3.675
Tao, Z., Han, L.H. and Zhuang, J.P. (2007), "Axial loading behavior of CFRP strengthened concrete filled steel tubular stub columns", *Adv. Struct. Eng.*, **10**(1), 37-46. https://doi.org/10.1260/136943307780150814
Wakabayashi, M. and Minami, K. (1990), "Application of high strength steel to composite structures", *Symposium on Mixed Structures, including New Materials, Brussels. IABSE*, Zurich, Switzerland.
Xiong, M.X. and Liew, J.Y.R. (2015), "Spalling behavior and residual resistance of fibre reinforced ultra-high performance concrete after elevated temperatures", *Mater. Construct.*, **65**(320), 1-10. https://doi.org/10.3989/mc.2015.00715
Xiong, M.X. and Liew, J.Y.R. (2016), "Mechanical behavior of ultra-high strength concrete at elevated temperatures and fire resistance of ultra-high strength concrete filled steel tubes", *Mater. Des.*, **104**, 414-427. https://doi.org/10.1016/j.matdes.2016.05.050
Xiong, M.X., Xiong, D.X. and Liew, J.Y.R. (2017a), "Axial performance of short concrete filled steel tubes with high- and ultra-high- strength materials", *Eng. Struct.*, **136**, 494-510. https://doi.org/10.1016/j.engstruct.2017.01.037
Xiong, M.X., Xiong, D.X. and Liew, J.Y.R. (2017b), "Behaviour of steel tubular members infilled with ultra high strength concrete", *J. Constr. Steel Res.*, **138**, 168-183. https://doi.org/10.1016/j.jcsr.2017.07.001
Xiong, M.X., Xiong, D.X. and Liew, J.Y.R. (2017c), "Flexural performance of concrete filled tubes with high tensile steel and ultra-high strength concrete", *J. Constr. Steel Res.*, **132**, 191-202. https://doi.org/10.1016/j.jcsr.2017.01.017
Xue, J.Y., Chen, Z.P., Zhao, H.T., Gao, L. and Liu, Z.Q. (2012), "Shear mechanism and bearing capacity calculation on steel reinforced concrete special-shaped columns", *Steel Compos. Struct., Int. J.*, **13**(5), 473-487. https://doi.org/10.12989/scs.2012.13.5.473
Yao, D.L., Jia, J.Q., Wu, F. and Yu, F. (2014), "Shear performance of prestressed ultra high strength concrete encased steel beams", *Constr. Build. Mater.*, **52**, 194-201. https://doi.org/10.1016/j.conbuildmat.2013.11.006

Zhu, W.Q., Meng, G.M. and Jia, J.Q. (2014), “Experimental studies on axial load performance of high-strength concrete short columns”, *Proceedings of the Institution of Civil Engineers-Structures and Buildings*, **167**(SB9), 509-519. https://doi.org/10.1680/stbu.13.00027

Zhu, W.Q., Jia, J.Q., Gao, J.C. and Zhang, F.S. (2016), “Experimental study on steel reinforced high-strength concrete columns under cyclic lateral force and constant axial load”, *Eng. Struct.*, **125**, 191-204. https://doi.org/10.1016/j.engstruct.2016.07.018

Zhu, W.Q., Jia, J.Q. and Zhang, J.G. (2017), “Experimental research on seismic behavior of steel reinforced high-strength concrete short columns”, *Steel Compos. Struct., Int. J.*, **25**(5), 603-615. https://doi.org/10.12989/scs.2017.25.5.603

*DL*

## Nomenclature

| | |
|---|---|
| $\alpha_M$ | the factor to reduce the moment resistance calculated from rectangular stress blocks |
| $A_a$ | the cross-sectional area of the encased steel section |
| $A_c$ | the cross-sectional area of the concrete |
| $A_s$ | the cross-sectional area of the longitudinal rebars |
| $b$ | the specimen cross-sectional width |
| $h$ | the specimen cross-sectional height |
| $c$ | the cover thickness of concrete |
| $e_a$ | the load eccentricity |
| $E_a$ | the elastic modulus of the encased steel section |
| $E_c$ | the elastic modulus of the concrete |
| $E_s$ | the elastic modulus of the longitudinal rebars |
| $f_{ay}$ | the strength of the encased steel section |
| $f_{ck}$ | the strength of the concrete |
| $f_{sy}$ | the strength of the longitudinal rebars |
| $h_n$ | the depth of the neutral axis from the centerline |
| $k$ | the amplification factor considering second-order effect |
| $L$ | the specimen height or span |
| $M_{pl}$ | the plastic moment resistance of flexural CES beams under bending |
| $N_{cr,eff}$ | the Euler’s buckling load |
| $N_{pl}$ | the axial capacity of the short CES columns under concentric axial loads |
| $N_u$ | the axial load |
| $s$ | the spacing of stirrups |
| $W_a$ | the plastic section modulus of the steel section |
| $W_{a,n}$ | the plastic section modulus of steel section within an area of $2h_n$ from centerline of composite section |
| $W_c$ | the plastic section modulus of the concrete section |
| $W_{c,n}$ | the plastic section modulus of the concrete section within the area of $2h_n$ from the centerline of the composite section |
| $W_s$ | the plastic section modulus of the longitudinal rebars |
| $W_{s,n}$ | the plastic section modulus of the longitudinal rebars within the area of $2h_n$ from the centerline of the composite section |
| $\beta$ | the equivalent moment factor |
| $\mu$ | the ductility index |
| $\Delta_{0.85}$ | the displacement corresponding to a load level after the load has dropped to 85% of its peak load |
| $\Delta_y$ | the displacement corresponding to the proportional limit |